In-plane permeability characterization of engineering textiles based on radial flow experiments: A benchmark exercise

D. May, A. Aktas, S.G. Advani, D.C. Berg, A. Endruweit, E. Fauster, S.V. Lomov, A. Long, P. Mitschang, S. Abaimov, et al.

In-plane permeability characterization of engineering textiles based on radial flow experiments: A benchmark exercise

D. May[a,*], A. Aktas[b], S.G. Advani[c], D.C. Berg[d], A. Endruweit[e], E. Fauster[f], S.V. Lomov[g], A. Long[e], P. Mitschang[a], S. Abaimov[h], D. Abliz[d], I. Akhatov[h], M.A. Ali[i], T.D. Allen[j], S. Bickerton[j], M. Bodaghi[k], B. Caglar[l], H. Caglar[l], A. Chiminelli[m], N. Correia[k], B. Cosson[n], M. Danzi[o], J. Dittmann[p], P. Ermanni[o], G. Francucci[q], A. George[r], V. Grishaev[h], M. Hancioglu[l], M.A. Kabachi[o], K. Kind[s], M. Deléglise-Lagardère[n], M. Laspalas[m], O.V. Lebedev[h], M. Lizaranzu[m], P.-J. Liotier[t], P. Middendorf[p], J. Morán[q], C.-H. Park[n], R.B. Pipes[u], M.F. Pucci[v], J. Raynal[w], E.S. Rodriguez[q], R. Schledjewski[f], R. Schubnel[w], N. Sharp[u], G. Sims[b], E.M. Sozer[l], P. Sousa[g], J. Thomas[i], R. Umer[i], W. Wijaya[j], B. Willenbacher[a], A. Yong[b], S. Zaremba[s], G. Ziegmann[d]

[a] *Institut für Verbundwerkstoffe GmbH, Germany*
[b] *Materials Division, National Physical Laboratory, United Kingdom*
[c] *Department of Mechanical Engineering and Center for Composite Materials, University of Delaware, USA*
[d] *Department of Polymer Materials and Plastics Engineering, Technische Universität Clausthal, Germany*
[e] *Faculty of Engineering, University of Nottingham, United Kingdom*
[f] *Processing of Composites Group, Montanuniversität Leoben, Austria*
[g] *Department of Mechanical Engineering, Katholieke Universiteit Leuven, Belgium*
[h] *Center for Design, Manufacturing and Materials, Skolkovo Institute of Science and Technology, Russia*
[i] *Khalifa University of Science and Technology (KUST), Abu Dhabi, United Arab Emirates*
[j] *Centre for Advanced Composite Materials, University of Auckland, New Zealand*
[k] *Composite Materials and Structures Group, INEGI, Portugal*
[l] *Department of Mechanical Engineering, KOÇ University, Turkey*
[m] *ITAINNOVA Instituto Tecnológico de Aragón, Spain*
[n] *Department of Polymers and Composites Technology & Mechanical Engineering, IMT Lille Douai, France*
[o] *Laboratory of Composite Materials and Adaptive Structures, ETH Zurich, Switzerland*
[p] *Institute of Aircraft Design, University of Stuttgart, Germany*
[q] *Institute of Research in Materials Science and Technology, Universidad Nacional de Mar del Plata, Argentina*
[r] *Faculty of Manufacturing Engineering Technology, Brigham Young University, USA*
[s] *Chair of Carbon Composites, Technische Universität München, Germany*
[t] *Mines Saint-Etienne, Université de Lyon, CNRS, UMR 5307 LGF, Centre SMS, Departement MPE, F-42023 Saint-Etienne, France*
[u] *Composites Manufacturing & Simulation Center, Purdue University, USA*
[v] *C2MA, IMT Mines Ales, Univ. Montpellier, Ales, France*
[w] *Institut de Soudure Group, France*

Although good progress was made by two international benchmark exercises on in-plane permeability, existing methods have not yet been standardized. This paper presents the results of a third benchmark exercise using in-plane permeability measurement, based on systems applying the radial unsaturated injection method. 19 par-ticipants using 20 systems characterized a non-crimp and a woven fabric at three different fiber volume contents, using a commercially available silicone oil as impregnating fluid. They followed a detailed characterization procedure and also completed a questionnaire on their set-up and analysis methods. Excluding outliers (2 of 20), the average coefficient of variation (c_v) between the participant's results was 32% and 44% (non-crimp and woven fabric), while the average c_v for individual participants was 8% and 12%, respectively. This indicates statistically significant variations between the measurement systems. Cavity deformation was identified as a major influence, besides fluid pressure/viscosity measurement, textile variations, and data analysis.

* Corresponding author.
E-mail address: david.may@ivw.uni-kl.de (D. May).

1. Introduction

Liquid Composite Molding (LCM) processes are employed for the manufacture of fiber reinforced polymer composites (FRPC), since they allow to efficiently manufacture components of different complexity and size at higher rates than autoclave processes. To obtain fast and complete saturation of the reinforcement with liquid resin in LCM, a suitable process design is desirable, which requires knowledge about material properties. The textile permeability is particularly important. It is defined by Darcy's law, which correlates the phase-averaged flow velocity v with the impregnating resin pressure gradient ∇P, its dynamic fluid viscosity μ, and the textile permeability$K$, which quantifies the conductance of the porous media for liquid flow (Eq. (1)).

$$v = -\left(\frac{K}{\mu}\right)\cdot\nabla P \tag{1}$$

The permeability of fiber structures, such as textiles, is generally direction-dependent and therefore described by a second-order tensor. Commonly, textile symmetry conditions are taken into account so that the tensor can be diagonalized, which leads to four remaining values describing flow in any direction within a fiber structure (assuming absence of coupling between in-plane and out-of-plane flow):

- Highest in-plane permeability (K_1), in-plane refers to the textile layer;
- Lowest in-plane permeability (K_2), oriented perpendicular to K_1;
- Orientation angle of K_1 (β), relative to the production direction of the material (0°);
- Out-of-plane permeability (K_3), oriented perpendicular to K_1 and K_2.

The present paper focuses on the characterization of the in-plane permeability (K_1, K_2 and β).

Despite the relevance of accurate permeability characterization for process efficiency, existing in-plane permeability characterization methods have not yet been standardized. Following several smaller regional benchmark studies [1–5], the results of the first truly international benchmark exercise on in-plane permeability measurement were published in 2011 [6]. In this exercise, same fabric was used by all participants, but no specifications were made regarding the measurement method and the test parameters. This resulted in a scatter of the measured permeability values of more than one order of magnitude. A second international benchmark exercise with a predefined measurement procedure [7] followed. The participants were required to apply an unsaturated linear injection method. In unsaturated linear injection of a fluid into a dry reinforcement sample, one-dimensional flow develops. The resulting flow front movement can be tracked, and the permeability along the specimen axis can be derived using a 1D formulation of Eq. (1). This benchmark exercise showed – for this specific test method – that by defining minimum requirements for equipment, measurement procedure and analysis, satisfactory reproducibility of data obtained using different systems can be achieved [8]. In-plane permeability characterization based on radial flow experiments is an alternative approach, where the test fluid is injected through a central injection gate into a tool cavity containing the reinforcement sample. Advantages of this approach are that only one test is required for full textile characterization including K_1, K_2 and β and that the possible influence of race-tracking on test results is reduced. Hence, it was agreed at the 13th International Conference on Flow Processes in Composite Materials (FPCM) in Kyoto (2016) to perform a third international benchmark exercise, focusing on unsaturated in-plane permeability characterization based on radial flow experiments. This benchmark exercise was organized by the Institut für Verbundwerkstoffe (IVW, Kaiserslautern, Germany), and strongly supported by the National Physical Laboratory (UK), the University of Nottingham, the University of Delaware (CCM), the Montanuniversität Leoben and KU Leuven as members of a steering committee. Furthermore, the organizers were strongly supported by the Department of Polymer Materials and Plastics Engineering at Clausthal University of Technology. Table 1 lists the participants of the presented benchmark exercise.

2. Materials & methods

2.1. Experimental set-up

2.1.1. Basic requirements

The presented benchmark focused on unsaturated in-plane permeability characterization based on radial flow. Taking into account the

Table 1
List of participants.

Participant	Institution	Department	Country
1	National University of Mar del Plata	Institute of Material Science and Technology	Argentina
2	Montanuniversität Leoben	Processing of Composites Group	Austria
3	Institut de Soudure – Composite Platform		France
4	IMT Lille Douai	Department of Polymers and Composites Technology & Mechanical Engineering	France
5	Institut für Verbundwerkstoffe GmbH	Manufacturing Science	Germany
6	Technsiche Universität Clausthal	Institute of Polymer Materials and Polymer Technology	Germany
7	Technische Universität München	Chair of Carbon Composites	Germany
8	University of Stuttgart	Institute of Aircraft Design	Germany
9	University of Auckland	Centre for Advanced Composite Materials	New Zealand
10	Institute of Science and Innovation in Mechanical and Industrial Engineering	Composite Materials and Structures Group	Portugal
11	Skolkovo Institute of Science and Technology	Center for Design, Manufacturing and Materials	Russia
12	ITAINNOVA	Materials and Components	Spain
13	ETH Zurich	Laboratory of Composite Materials and Adaptive Structures	Switzerland
14	Koc University	Department of Mechanical Engineering	Turkey
15	Khalifa University of Science and Technology	Department of Aerospace Enigneering	UAE
16	National Physical Laboratory	Materials Division	UK
17	Nottingham University	Faculty of Engineering	UK
18	Brigham Young University	Faculty of Manufacturing Engineering Technology	USA
19	Purdue University	Composites Manufacturing & Simulation Center	USA

guidelines of the 2nd international benchmark on in-plane permeability characterization based on the linear flow method [7], basic requirements for the experimental set-up, used materials and the measurement procedure were specified for all participants:

- A stack of textile layers is compressed between two rigid mold surfaces at constant gap height (as illustrated in Fig. 1).
- A test fluid is injected through a central circular hole (12 mm diameter), resulting in a two-dimensional flow pattern (typically an ellipse). The injection hole has to be punched into the textile.
- An unsaturated measurement principle is applied, i.e. flow front progression is tracked.
- No vacuum is applied.

2.1.2. Individual set-ups of the participants

Within the constraints of the stated basic requirements, a wide variety of designs of experimental set-ups was used by the participants. Table 2 gives an overview of the most important characteristics of the systems. Except for system #13, which is based on constant flow rate, all systems work with a constant injection pressure.

2.2. Materials

Two different reinforcement textiles were tested:

- A biaxial (± 45°) glass fiber non-crimp fabric (NCF) from Saertex (X-E-444 g/m^2) with a nominal areal weight of 444 g/m^2 (217 g/m^2 in +45° and in −45° direction and additionally 1 g/m^2 and 2 g/m^2 in 0° and 90°, respectively, for stabilization) as well as 6 g/m^2 polyester stitching yarn (76 dtex) with a warp pattern at a stitch length of 2.6 mm and a gauge length of 5 mm.
- A twill weave (2/2) glass fiber woven fabric (WF) from Hexcel (01102) with a nominal areal weight of 295 g/m^2 equally distributed in weft and warp direction. Nominal construction is 7 yarns/cm in weft and warp direction.

Both fabrics are nominally balanced. The actual construction of the WF is somehow different in warp and weft direction: ends (warp) count is 7.13 yarns/cm, picks (weft) count is 7.00 yarns/cm. For the NCF the bundle count is 4.2 bundles/cm in production direction and 4.1 bundles/cm perpendicular to it. Hence, the 45°-orientation is quite accurate. Table 3 lists further details on the geometry of the textiles. The values were averaged based on the results of 30 single measurements, whereas the width of the yarns was measured with a distance of 1.5 mm (WF) and 3.0 mm (NCF) respectively. For both textiles, all participants in this study received material from the same batch, in order to minimize the influence of potential manufacturing variations on the benchmark results. Fig. 2 shows surface images of both textiles.

The silicone oil XIAMETER® PMX-200 SILICONE FLUID 100CS supplied by Dow Corning was used as test fluid for permeability measurement. Its viscosity is approximately 100 mPa·s at room temperature. In order to minimize possible variations induced by the fluid viscosity, the silicone oil was procured batch-wise. For each of the ten batches used by different participants, the viscosity was centrally measured at TU München in a temperature range from 15 °C to 40 °C using an Anton Paar MCR 302 rheometer. This silicone oil was used by all participants except for participant #12, who used polymer solution in water as a test fluid, as the silicone oil caused problems with their sensors for flow front monitoring.

2.3. Test plan

The participants were asked to perform measurements on the non-crimp fabric (NCF) and the woven fabric (WF) using the parameters (cavity height, number of layers, injection pressure, and number of repetitions) specified Table 4. While the number of layers can have an influence on measured permeability, due to effects of nesting between layers and edge effects at the fabric-tool interface [18], such influence is assumed to be negligible for this benchmark, as eight layers or more are used. All measurements were performed at a single cavity height, but different number of layers to minimize the effort for spacer frame manufacturing. The specified numbers of layers, the nominal areal weights of the tested textiles, and the specified cavity heights define the target level of fiber volume contents (V_f), shown in Table 4.

Based on exploratory tests, the target level of fluid injection pressure (Table 4) was specified in order to avoid possible effects of injection pressure on measured permeabilities. The definition of target pressure is especially relevant for radial-flow experiments, because the high pressure gradient may cause fiber displacement at the inlet hole. The specified pressure values were also chosen to obtain reasonable test times between one and five minutes. No vacuum was applied at the outlet during the tests.

For each of the two fabric materials, three series of experiments were specified, whereas each series comprised five experiments at repeatable conditions in order to add statistical significance to the results.

2.4. Data analysis

Analysis of the raw data acquired in the tests, i.e. fitting of an ellipse to measured points on the flow front and calculation of permeability values based on the process conditions and the development of the flow ellipse geometry with time, was performed by each individual participant for their respective data. Table 5 sums-up the analysis methods employed by the participants. It is to be noted that all methods used here (Chan/Hwang [19], Adams Rebenfeld [18,20–22] and Weitzenboeck et al. [23,24]) are based on different formulations of the same approach, transformation of an elliptical flow front shape to an equivalent isotropic co-ordinate system. However, these methods differ in the particular mathematical approach chosen for this transformation.

2.5. Sample preparation

For preparation of the test specimens, all participants were asked to follow these pre-defined steps:

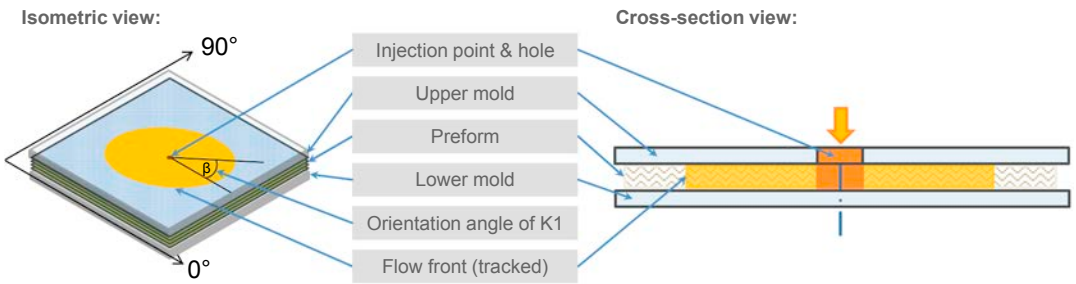

Fig. 1. Schematic illustration of the radial injection approach which is the focus of this benchmark exercise. (For interpretation of the references to colour in this figure legend, the reader is referred to the web version of this article.)

Table 2
Details of the individual set-ups.

Participant #	Sample size in mm[2]	Length to width ratio	Tool material (top/bottom)	Flow detection	Monitoring injection pressure[1]	Monitoring temperature[2]	Liter-ature
1	51,129	1:1	glass/metal	optical	none	pressure vessel	
2a[3]	112,687	3:4	glass + steel reinforcement/steel	optical	feed line	feed line	[9,10]
2b[3]	215,812	1:1	aluminum/aluminum	capacitive	prop. valve	tool	[5]
3	95,586	1:1	aluminum/aluminum	pressure (6 sensors)	tool	room	
4	160,000	1:1	steel/PMMA	optical	feed line	room	
5	215,568	1:1	aluminum/aluminum	capacitive	None	tool	[5,11]
6	62,387	1:1	glass + metal reinforcement/metal	optical	feed line	feed line	[10,12]
7	78,287	circular	glass/aluminum	optical	feed line	feed line	[28]
8	89,887	1:1	PMMA/aluminum	optical	feed line	pressure vessel + tool	
9	72,900	1:1	glass/aluminum	optical	feed line	tool	[13]
10	80,384	circular	metal/metal	pressure (64 sensors)	tool	tool	
11	7,741	circular	PMMA/PMMA	optical	feed line	feed line	
12	107,187	3:4	steel/steel	dielectrical (22 sensors)	feed line	tool	
13	193,487	1:1	metal/metal	pressure	tool	n/a[4]	[14]
14	72,787	1:1	glass-aluminum sandwich/ aluminum	optical	feed line	feed line	
15	31,303	circular	metal/glass	optical	feed line	feed line	[15]
16	89,887	1:1	glass + aluminum reinforcement/ metal	optical	tool	tool	
17	125,551	circular	aluminium/aluminum	pressure (6 sensors)	tool	pressure vessel	[16]
18	22,387	1:1	PMMA/PMMA	optical	prop. valve	Tool	
19	40,000	1:1	PMMA/PMMA	optical	feed line	pressure vessel	

[1, 2] Refers to the location of the sensor from which the values are used for calculation.
[3] Participant #2 participated in the benchmark with 2 different systems.
[4] This was the only system in the benchmark working with constant flow rate instead of constant injection pressure.

Table 3
Variations in textile geometry.

Non-crimp fabric	Bundle width ($\bar{x}$)	1.66 ± 0.08 mm
	Stitches distance	5.23 ± 0.04 mm
	Bundle gap	0.32 ± 0.01 mm
Woven fabric	Warp width ($\bar{x}_{warp}$)	1.21 ± 0.05 mm
	Weft width ($\bar{x}_{weft}$)	1.47 ± 0.05 mm
	Warp gap	0.25 ± 0.06 mm

Table 4
Test plan.

Test series	Material	No. of layers	Fiber volume content (V_f) in %	Injection pressure (gauge) in MPa	No. of repeats	Cavity height in mm
NCF – $V_{f,1}$	NCF	8	46.4	0.1	5	3.00
NCF – $V_{f,2}$		9	52.2	0.2		
NCF – $V_{f,3}$		10	58.0	0.4		
WF – $V_{f,1}$	WF	12	46.3	0.1		
WF – $V_{f,2}$		13	50.1	0.2		
WF – $V_{f,3}$		14	54.0	0.4		

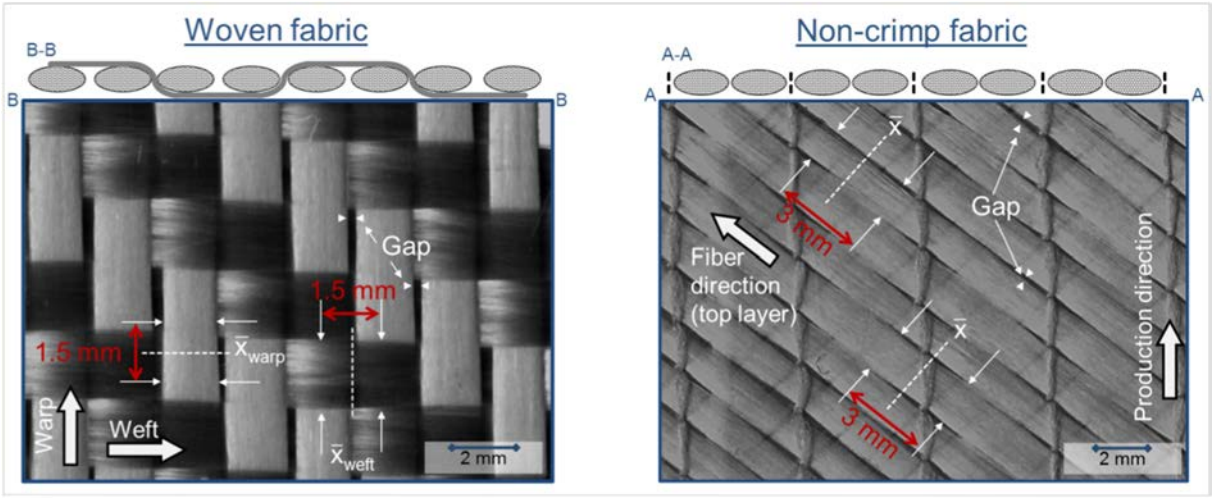

Fig. 2. Images of the textiles characterized in this benchmark study. (For interpretation of the references to colour in this figure legend, the reader is referred to the web version of this article.)

Table 5

Analysis methods implemented by the participants.

Participant #	Algorithm for analysis[1]	Evaluation method[2]	Ellipse-fitting centered[3]	Method of pressure consideration[4]
1	Chan/Hwang	Global Method	yes	average
2a	Adams/Rebenfeld	Global Method	yes	average
2b	Adams/Rebenfeld	Global Method	yes	average
3	n/a	Single Step Method	no	target
4	Chan/Hwang	Global Method	yes	average
5	Adams/Rebenfeld	Global Method	yes	target
6	Modified[5] Chan/Hwang	Global Method	yes	average/single value
7	Adams/Rebenfeld	Elementary Method	yes	average
8	Adams/Rebenfeld	Global Method	no	average
9	Weitzenböck et al.	Reference Time Step Method	yes	single value
10	Adams/Rebenfeld	Global Method	yes	average
11	Chan/Hwang	Global Method	no	average
12	n/a	Global Method	yes	average
13	Chan/Hwang	Elementary Method	yes	single value
14	Weitzenböck et al.	Global Method	yes	average
15	Weitzenböck et al.	Reference Time Step Method	no	average
16	Weitzenböck et al.	Global Method	yes	average
17	Weitzenböck et al.	Elementary Method	yes	average
18	Adams/Rebenfeld	Global Method	yes	average
19	Chan/Hwang	Global Method	yes	target

[1] For detailed explanation we refer to these publications: Chan/Wang: [19]; Adams/Rebenfeld: [18,20–22]; Weitzenböck et al. [23,24].

[2] For detailed explanation we refer to Ferland et al. [17].

[3] When fitting an ellipse to the flow data there are two possibilites: Either fix the ellipse-center to the injection point (yes) or to allow the location of the ellipse center to deviate from the injection point (no).

[4] Refers to the way how injection pressure is considered in permeability calculation → Average: All captured values are averaged; single value: for every time step the currently captured pressure value is considered; target: the target injection pressure is assumed.

[5] Chan model was modified to correct an error: the inlet radius is stated to be falsely transformed, Fauster et al. [4].

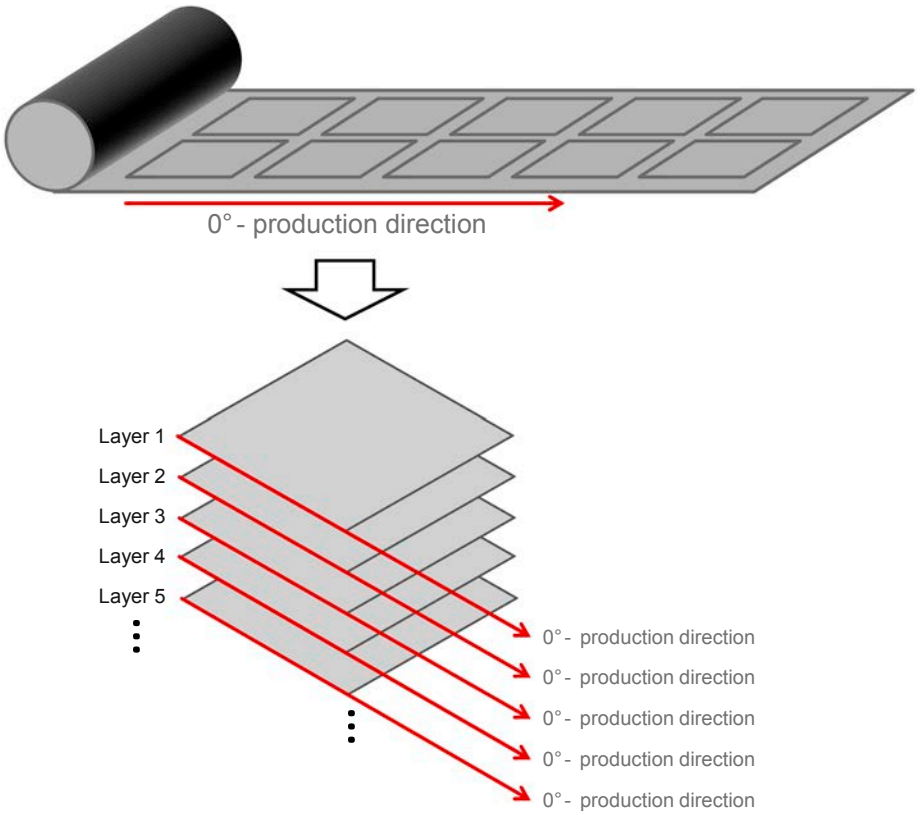

Fig. 3. Cutting and stacking of the samples – all layers have identical orientation. (For interpretation of the references to colour in this figure legend, the reader is referred to the web version of this article.)

In the first step, the individual fabric layers were cut out of the material at the required size and shape (determined by each participant's injection tool geometry) and then stacked at identical orientation according to Fig. 3. The number of layers in each test specimen was defined by the test plan (Table 4).

In the second step, the inlet hole, a specific characteristic of radial injection tests, was punched into the stack. A diameter of 12 mm was pre-defined. The accuracy of the inlet hole diameter is crucial for a precise measurement and therefore special care must be taken when preparing it. Hence, punching was defined as requirement because

cutting the hole may result in yarns being displaced. Also, punching was performed on the complete stacks, because if the hole is punched into the individual layers, the following stacking process can lead to offset and therefore insufficient accuracy.

In the third step, each specimen was weighed for calculation of the actual fiber volume content.

2.6. Evaluation of cavity deformation

The participants were asked to evaluate experimentally the cavity deformation in their injection tool and the corresponding deviation from the target cavity height of 3.00 mm. For this purpose, blocks of plasticine, liquid metal filler (metal epoxy), or similar materials were placed in the tool cavity at five points according to the scheme shown in Fig. 4, where P5 is located as close as possible to the inlet. The tool was closed, compressing the material blocks to a thickness corresponding to the cavity height. After opening of the tool, the thickness of the material blocks was measured to determine the cavity height. Two cases were considered. In a first test the empty and non-pressurized cavity was checked. In a second case the tool was filled with the NCF at the highest tested fiber volume content (58%) with cutouts for the plasticine. From compression tests it is known that the NCF at a V_f of 58% results in the highest textile compaction pressure of all tests. It must be noted that textile compression pressure is the dominant component of overall pressure, because it easily exceeds the maximum injection pressure of 0.4 MPa and acts on the complete surface. While the obtained deformations do not fully reflect the actual deformation during the experiments, they give an good impression of the tendency of a system to deviate from the target cavity thickness. From the five values per case, an average effective cavity height was calculated and compared to the target cavity height and the parallelity of the upper and lower mold halves was assessed. While more complex methods for deformation analysis, exist, this simple approach exhibits a high robustness and is easily manageable for all participants because it requires no specific technology.

3. Results

Tables 6 and 7 list the main results of all participants. It should be noted that participant #2 acquired permeability data using two different set-ups (see Table 2), while participants #7 and #17 provided two data sets, one as measured, and one with correction for deviations in cavity height. Furthermore, participant #6 only provided data, in which V_f was corrected with the actual cavity height, as their system provides an online cavity height measurement during the test.

Figs. 5 and 6 summarize the measured permeability values for the NCF and the WF, respectively. Each figure contains two diagrams, showing the highest (K_1) and lowest (K_2) in-plane permeability value (logarithmic scale) as a function of the V_f. In each diagram, the blue diamonds, the red squares and the green triangles show the results for the lowest ($V_{f,1}$), intermediate ($V_{f,2}$) and highest ($V_{f,3}$) target V_f, respectively. Each data point represents the arithmetic average of the five repeat measurements conducted by each participant. The error bars represent the standard deviation for permeability and V_f. Deviations from the target V_f are induced by areal weight variations, which were taken into account by weighing every specimen and calculating the individual V_f for every test. In these figures, calculation of V_f is based on target values for the cavity height, not on the actually measured values (except for participant #6, because an online-correction is implemented in their system).

In the diagrams, almost all data sets lie within a cluster at each nominal V_f. Series #1 and #19 are exceptions for each data point, i.e. for both textiles, K_1 and K_2, and for each V_f (data set #1 is incomplete, if they are not marked in the diagram then there was no data available). The fact that the relative position of the data sets #1 and #19 to the cluster is constant indicates a systematic deviation. Therefore, these data sets were excluded from further statistical analysis since they are obvious outliers. On the other hand, this means that 18 of the 20 data sets are included in the cluster and can be considered for statistical analysis. Possible effects that may contribute to the observed deviation are discussed in the following sections.

Each cluster covers a range of about two percentage points of V_f (e.g. 46% to 48%). While these variations in V_f can have a strong effect on the permeability, there is no correlation of permeability and V_f within each cluster, indicating that other effects causing variation in the measured permeability values are dominant.

Within each cluster, the coefficient of variation (c_v) of the permeability values was calculated according to Eq. (2), with σ being the standard deviation and $\bar{x}_{arith}$ being the arithmetic average

$$cv = \frac{\sigma}{\bar{x}_{arith}} \tag{2}$$

The results listed in Table 8 show that the average for the c_v was 32.2% and 43.9% for the NCF and the WF, respectively. The higher average c_v for the WF mainly results from K_2, which shows relatively high variation. This might results from the comparably small value, leading to errors induced by issues measurement resolution for flow front progression.

The target of the benchmarking efforts is to reach a point at which the variation between the results gained with different systems is no

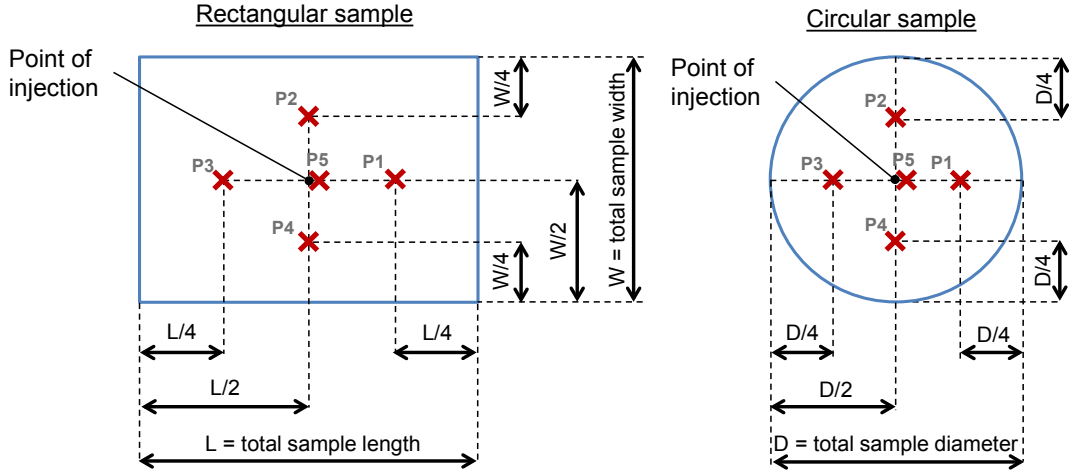

Fig. 4. Positions for measurement of the actual cavity height. (For interpretation of the references to colour in this figure legend, the reader is referred to the web version of this article.)

Table 6
Results for the permeability for the NCF.

Partici-pant #		Fiber volume content in % (± c_v)	K_1 in 10^{-11} m^2 (± c_v)	K_2 in 10^{-11} m^2 (± c_v)	Orientation angle of K_1
1	$V_{f,1}$	46.1 (± 1.4%)	44.2 (± 13.8%)	38.0 (± 15.8%)	6.6
	$V_{f,2}$	51.2 (± 1.3%)	24.0 (± 15.8%)	21.5 (± 17.8%)	−33.0
	$V_{f,3}$	58.8 (± 0.5%)	17.7 (± 3.3%)	13.6 (± 7.5%)	−29.0
2a	$V_{f,1}$	47.0 (± 0.1%)	6.32(± 5.9%)	4.85 (± 3.0%)	13.0
	$V_{f,2}$	52.9(± 0.1%)	3.77(± 4.8%)	2.81(± 6.4%)	4.6
	$V_{f,3}$	58.7(± 0.2%)	2.16 (± 2.0%)	1.56 (± 4.2%)	3.9
2b	$V_{f,1}$	47.0 (± 0.1%)	4.80 (± 11.7%)	3.70 (± 11.6%)	−4.97
	$V_{f,2}$	52.9(± 0.1%)	3.14(± 1.9%)	2.30(± 4.0%)	−0.24
	$V_{f,3}$	58.7(± 0.0%)	1.39(± 5.8%)	1.02(± 4.9%)	6.12
3	$V_{f,1}$	47.3(± 0.1%)	5.82 (± 5.8%)	5.32(± 6.1%)	n/a
	$V_{f,2}$	53.2(± 0.1%)	3.08(± 3.2%)	3.02(± 3.6%)	n/a
	$V_{f,3}$	59.2(± 0.1%)	1.68(± 5.8%)	1.58(± 10.4%)	n/a
4[1]	$V_{f,1}$	47.0(± 0.2%)	3.79(± 3.4%)	2.99(± 3.6%)	−3.6
	$V_{f,2}$	52.7(± 0.1%)	3.08(± 8.0%)	2.43(± 9.7%)	−4.1
	$V_{f,3}$	n/a	n/a	n/a	n/a
5	$V_{f,1}$	47.0(± 0.1%)	6.78(± 4.2%)	5.21(± 4.3%)	1.8
	$V_{f,2}$	53.0(± 0.1%)	3.62(± 5.0%)	2.70(± 7.4%)	3.4
	$V_{f,3}$	58.8(± 0.1%)	1.59(± 8.6%)	1.12 (± 9.1%)	4.1
6	$V_{f,1}$	46.4(± 0.4%)	5.75(± 4.5%)	4.63(± 3.5%)	8.5
	$V_{f,2}$	52.3(± 0.2%)	3.07(± 10.6%)	2.39(± 9.3%)	10.1
	$V_{f,3}$	58.0(± 0.4%)	1.36(± 5.3%)	1.00(± 7.6%)	7.4
7a	$V_{f,1}$	47.0(± 0.3%)	2.72(± 7.9%)	1.95(± 9.2%)	11.5
	$V_{f,2}$	52.9(± 0.7%)	1.53(± 8.6%)	1.09(± 10.2%)	7.4
	$V_{f,3}$	58.8(± 0.8%)	0.996(± 10.4%)	0.663(± 6.7%)	13.1
7b	$V_{f,1}$	44.2(± 0.3%)	2.72(± 7.9%)	1.95(± 9.2%)	11.5
	$V_{f,2}$	50.2(± 0.7%)	1.53(± 8.6%)	1.09(± 10.2%)	7.4
	$V_{f,3}$	54.9(± 0.8%)	0.996(± 10.4%)	0.663(± 6.7%)	13.1
8	$V_{f,1}$	47.0(± 0.1%)	4.27(± 9.1%)	3.50 (± 7.2%)	9.6
	$V_{f,2}$	53.1(± 0.2%)	2.34(± 3.8%)	1.88(± 4.7%)	8.7
	$V_{f,3}$	58.9(± 0.1%)	1.34(± 7.4%)	1.03(± 11.0%)	11.8
9	$V_{f,1}$	47.3(± 0.2%)	6.55(± 7.0%)	4.61(± 11.4%)	−26.3
	$V_{f,2}$	53.2(± 0.1%)	3.52(± 5.4%)	2.46(± 10.5%)	−27.6
	$V_{f,3}$	59.1(± 0.2%)	1.68(± 6.7%)	1.04(± 7.9%)	−26.7
10	$V_{f,1}$	47.4(± 0.3%)	2.48(± 11.6%)	1.92(± 12.0%)	29.2
	$V_{f,2}$	53.2(± 0.1%)	1.65(± 10.9%)	1.26(± 5.6%)	20.5
	$V_{f,3}$	59.3(± 0.3%)	1.17(± 24.0%)	0.832(± 18.9%)	29.7
11	$V_{f,1}$	48.0(± 0.3%)	5.98(± 2.5%)	5.10(± 4.2%)	20.0
	$V_{f,2}$	54.0(± 0.3%)	2.75(± 5.4%)	2.18(± 5.3%)	18.5
	$V_{f,3}$	60.1(± 0.5%)	0.953(± 6.7%)	0.75(± 7.9%)	13.0
12	$V_{f,1}$	47.1(± 0.5%)	7.24(± 7.3%)	5.53(± 7.8%)	−17.7
	$V_{f,2}$	53.1(± 0.5%)	4.22(± 1.7%)	3.11(± 7.1%)	−19.4
	$V_{f,3}$	59.0(± 0.6%)	1.94(± 14.2%)	1.32(± 13.2%)	−23.7
13	$V_{f,1}$	46.6(± 1.4%)	5.18(± 15.3%)	4.20(± 14.7%)	22.8
	$V_{f,2}$	52.8(± 0.3%)	2.86(± 5.6%)	2.41(± 7.4%)	10.4
	$V_{f,3}$	58.7(± 0.1%)	1.56(± 13.2%)	1.32(± 7.4%)	4.0
14	$V_{f,1}$	46.6(± 0.3%)	7.26(± 3.9%)	5.65(± 4.0%)	8.1
	$V_{f,2}$	52.5(± 0.1%)	5.59(± 24.5%)	4.17(± 29.5%)	9.3
	$V_{f,3}$	58.3(± 0.1%)	3.25(± 6.3%)	2.39(± 9.3%)	5.1
15	$V_{f,1}$	47.3(± 0.1%)	8.11(± 7.0%)	5.87(± 6.8%)	16.0
	$V_{f,2}$	53.2(± 0.1%)	3.08 (± 6.2%)	2.10(± 5.9%)	13.8
	$V_{f,3}$	59.2(± 0.1%)	1.57(± 4.3%)	1.02(± 6.6%)	16.0
16	$V_{f,1}$	47.4(± 0.1%)	5.46(± 5.2%)	4.30(± 4.7%)	−3.1
	$V_{f,2}$	53.3(± 0.1%)	2.89(± 3.7%)	2.36(± 3.1%)	9.7
	$V_{f,3}$	59.2(± 0.1%)	1.81(± 8.5%)	1.60(± 9.6%)	7.2
17a	$V_{f,1}$	47.4(± 0.1%)	6.75(± 5.7%)	5.12(± 5.2%)	−17.2
	$V_{f,2}$	53.3(± 0.1%)	4.39(± 3.0%)	3.30(± 3.0%)	−14.2
	$V_{f,3}$	59.3(± 0.1%)	3.20(± 2.7%)	2.40(± 10.3%)	−18.2
17b	$V_{f,1}$	46.6(± 0.1%)	6.85(± 5.7%)	5.20(± 5.2%)	−17.2
	$V_{f,2}$	50.2(± 0.1%)	4.68(± 3.0%)	3.52(± 3.0%)	−14.2
	$V_{f,3}$	52.6(± 0.1%)	3.73(± 2.7%)	2.79(± 10.2%)	−18.2
18	$V_{f,1}$	47.0(± 0.9%)	3.97(7.8 ± %)	3.05(± 8.9%)	−42.4
	$V_{f,2}$	52.7(± 0.3%)	2.04(9.7 ± %)	1.49(± 13.0%)	31.3
	$V_{f,3}$	58.6(± 0.3%)	1.06(8.7 ± %)	0.758(± 10.8%)	35.0

(*continued on next page*)

Table 6 (*continued*)

Partici-pant #		Fiber volume content in % (± c_v)	K_1 in 10^{-11} m^2 (± c_v)	K_2 in 10^{-11} m^2 (± c_v)	Orientation angle of K_1
19	$V_{f,1}$	48.4(± 0.3%)	196(29.0 ± %)	149(± 25.0%)	40.7
	$V_{f,2}$	54.4(± 0.2%)	111(11.3 ± %)	91.7(± 9.5%)	29.2
	$V_{f,3}$	60.5(± 0.2%)	74.9(12.2 ± %)	62.2(± 20.4%)	38.0

[1] These values have been revised after first results presentation at FPCM14 as a unit conversion error was identified in the analysis software of the participant.

larger than the variation between the results gained on a single system. On average, the c_v for individual data sets was 7.8% and 12.2% for the NCF and the WF, respectively. Hence, there is further potential for improvement. This leads to the question which sources of variation can be identified based on the results and the information provided by the participants. In Section 4, different potential sources are discussed in detail.

In addition to the permeability values K_1 and K_2, the orientation angle β of K_1 relative to the fiber directions values was determined in the tests. Fig. 7 shows the results for both textiles at each of the three nominal V_f. Each blue line in the graphs represents the β, averaged out of the five tests for each individual participant. The red dashed line shows the average of all participants.

Both textiles show an average orientation close to 0°. Yet, there is significant variation between the participants, especially for the NCF. A possible explanation might be given by the degree of anisotropy of permeability, which is defined as the ratio of K_2 to K_1. The closer this ratio is to one, the more circular the flow front is. As the orientation angle is derived from the ellipse fitted to the flow front, a near-circular shape increases the influence of irregularities in the flow front shape. Table 9 lists the degrees of anisotropy for both textiles. It shows low anisotropy (≥ 0.75) for the NCF. As the relative length of the half-axis corresponds to $\sqrt{K_1}/\sqrt{K_2}$, a degree of anisotropy of 0.75 means that the short half-axis is only about 13% shorter than the long half-axis. Hence, this might explain the high variation concerning β. As there are no significant differences in fiber bundle geometry for the two main fiber directions (see Table 3), the slight anisotropy of the NCF is likely to be caused by the presence of stitching, oriented in the production direction. On the other side, the WF shows relatively high anisotropy (≤ 0.21). This presumably results from the deviations from the balanced fabric construction, which are listed in Table 3 and visible in Fig. 2.

In summary, the results show that for radial flow measurements the error in orientation angle determination increases with decreasing anisotropy. The variability is small when the anisotropy is high. This seems acceptable, since the relevance of the orientation angle decreases as the flow front becomes more circular.

Both orientation angle and anisotropy did not show a clear dependence on V_f.

4. Discussion

4.1. Influence of cavity deformation

The data listed in Table 8 clearly shows that the variation between the results of the different institutions increases with increasing V_f. This influence of V_f is presumably related to increasing cavity deformation resulting from increasing textile compression and also from increasing injection pressure. While relatively stiff systems remain closer to the target cavity height of 3.00 mm, the less stiff ones show increasing cavity height, presumably related to tool deflection. This leads to apparently higher in-plane permeability values. As a result, the deviations of the permeability data obtained by the participants increase with the level of V_f.

To estimate the influence of deformation in detail, Fig. 8 shows the results of the cavity height measurements. The figure contains a green, dashed line at 2% deviation showing the originally proposed acceptable limit for deviation, which was defined based on the guideline for Benchmark II [7].

The results show that 10 out of 20 systems show a deviation greater than 2% when the textile is compacted in the cavity. Relating this data to the materials used for the systems (Table 2), one can see that out of the seven full metal systems two show deviation larger 2% while this was the case for eight out of thirteen systems which were fully or partially made of glass or PMMA. This indicates that neither usage of full metal system guarantees satisfying stiffness, nor usage of glass or PMMA necessarily leads to insufficient stiffness, although it tends to make systems more prone to deflection. Hence, it can be concluded that appropriate tool design is the key to minimizing cavity height variations.

The impact of the deformation on the variation of the results becomes clear when only the 10 systems with a deviation from target cavity height smaller than 2% are considered for statistical analysis: In this case, the average c_v reduces to 23% and 34% for the NCF and the WF, respectively. This gets close to the average c_v found in Benchmark II which was approximately 20% for systems with deviation between actual and target cavity height smaller than 2%. Yet, it has to be noted that Benchmark II was conducted with a different textile and hence a direct comparison is not possible.

When considering cavity height deviation, it is important to distinguish between parallel and non-parallel deviation. The latter, which can be caused by a pressure-induced deflection or a parallelism issue between top and bottom molds, is practically impossible to correct because it results in a non-uniformly distributed V_f over the sample area and depends, among other factors, on the compaction behavior of the textile in dry and wet state as well as the fluid pressure. Both are not constant during the experiment, as the flow front propagates. It must be noted that set-ups for radial injection tests are quite prone to pressure-induced deflection, due to the central injection and the resulting high pressure gradient. On the other side a known (measured) parallel deviation from the target can be accounted for when calculating the effective V_f. Table 10 shows the normalized non-parallelity factor ω of the deformation for all participants (Eq. (3)). It is defined as the ratio of σ_h, the standard deviation of the cavity height at the five measurement points (with textile in cavity) to θ_h, the arithmetic average of the five values.

$$\omega = \frac{\sigma_h}{\theta_h} \tag{3}$$

Some participants observed relatively large average deviations, but only small non-parallel deformation, so that applying a correction to the fiber volume content was possible (#7 and #17 in Tables 6 and 7).

4.2. Influence of fluid pressure

The injection pressure to be used in the tests was pre-defined (Table 4) in order to minimize possible influences of pressure on permeability results. Among the 20 systems used in the benchmark, 2 provided a pressure sensor located directly at the proportional valve of the pressure vessel, 11 had a sensor somewhere in the feed line between oil reservoir and tool, and 5 had a tool-mounted sensor. The rest used the nominal pressure value to which the proportional valve is set for calculation. Two basic possibilities for an influence of fluid pressure on the calculated permeability are given.

Table 7
Results for the permeability for the WF.

Partici-pant #		fiber volume content in % (± c_v)	K_1 in 10^{-11} m^2 (± c_v)	K_2 in 10^{-11} m^2 (± c_v)	Orientation angle of K_1
1	$V_{f,1}$	n/a	n/a	n/a	n/a
	$V_{f,2}$	n/a	n/a	n/a	n/a
	$V_{f,3}$	n/a	n/a	n/a	n/a
2a	$V_{f,1}$	45.5(± 0.2%)	5.28(± 13.0%)	0.993(± 9.9%)	0.79
	$V_{f,2}$	49.3(± 0.1%)	3.87(± 21.0%)	0.554(± 22.7%)	1.23
	$V_{f,3}$	53.0(± 0.1%)	2.86(± 15.5%)	0.348(± 20.8%)	0.91
2b	$V_{f,1}$	45.7(± 0.0%)	4.85(± 8.1%)	1.02(± 23.1%)	−0.41
	$V_{f,2}$	49.5(± 0.1%)	2.83(± 2.7%)	0.422(± 11.2%)	−0.31
	$V_{f,3}$	53.1(± 0.1%)	1.86(± 17.8%)	0.223(± 21.0%)	0.94
3[1]	$V_{f,1}$	45.6(± 0.1%)	7.24(± 10.4%)	1.32(± 5.7%)	n/a
	$V_{f,2}$	49.4(± 0.1%)	5.00(± 10.1%)	0.826(± 12.7%)	n/a
	$V_{f,3}$	53.2(± 0.1%)	2.64(± 7.8%)	0.424(± 23.1%)	n/a
4[2]	$V_{f,1}$	46.1(± 0.1%)	3.59(± 10.8%)	0.507(± 12.9%)	−0.12
	$V_{f,2}$	50.0(± 0.1%)	3.17(± 10.1%)	0.444(± 16.7%)	−0.67
	$V_{f,3}$	n/a	n/a	n/a	n/a
5	$V_{f,1}$	45.4(± 0.1%)	7.26(± 4.2%)	1.05(± 7.3%)	−0.90
	$V_{f,2}$	49.3(± 0.2%)	4.52(± 8.8%)	0.524(± 8.9%)	0.17
	$V_{f,3}$	53.1(± 0.2%)	2.64(± 6.6%)	0.279(± 19.5%)	0.88
6	$V_{f,1}$	45.3(± 0.3%)	6.35(± 10.4%)	1.29(± 10.3%)	−0.78
	$V_{f,2}$	49.2(± 0.2%)	4.03(± 15.3%)	0.616(± 17.0%)	−1.17
	$V_{f,3}$	52.7(± 0.7%)	2.69(± 6.2%)	0.374(± 16.3%)	−0.01
7a	$V_{f,1}$	45.7(± 0.6%)	3.94(± 13.6%)	0.389(± 13.2%)	0.36
	$V_{f,2}$	49.5(± 0.4%)	2.90(± 12.2%)	0.260(± 7.9%)	−0.12
	$V_{f,3}$	53.3(± 0.2%)	2.26(± 10.7%)	0.176(± 19.6%)	0.77
7b	$V_{f,1}$	43.7(± 0.6%)	3.94(± 13.6%)	0.389(± 13.2%)	0.36
	$V_{f,2}$	46.3(± 0.4%)	2.90(± 12.2%)	0.260(± 7.9%)	−0.12
	$V_{f,3}$	49.8(± 0.2%)	2.26(± 10.7%)	0.176(± 19.6%)	0.77
8	$V_{f,1}$	45.6(± 0.0%)	5.36(± 7.3%)	1.08(± 6.2%)	0.53
	$V_{f,2}$	49.7(± 0.1%)	3.10(± 7.5%)	0.543(± 14.9%)	1.29
	$V_{f,3}$	53.3(± 0.0%)	1.83(± 8.1%)	0.290(± 2.0%)	1.08
9	$V_{f,1}$	45.2(± 0.1%)	7.88(± 30.5%)	2.32(± 28.3%)	−13.68
	$V_{f,2}$	49.1(± 0.1%)	7.09(± 4.4%)	1.52(± 11.1%)	0.25
	$V_{f,3}$	52.9(± 0.1%)	4.67(± 26.5%)	0.897(± 40.0%)	1.92
10	$V_{f,1}$	46.0(± 0.1%)	2.97(± 21.7%)	0.506(± 13.1%)	3.96
	$V_{f,2}$	49.3(± 0.3%)	2.33(± 7.3%)	0.363(± 9.7%)	3.60
	$V_{f,3}$	53.5(± 0.2%)	1.38(± 10.4%)	0.211(± 14.1%)	2.56
11	$V_{f,1}$	46.3(± 0.3%)	5.76(± 13.7%)	1.41(± 16.5%)	5.09
	$V_{f,2}$	50.3(± 0.1%)	3.39(± 9.6%)	0.852(± 9.0%)	1.95
	$V_{f,3}$	54.3(± 0.3%)	2.53(± 19.3%)	0.520(± 12.6%)	3.99
12	$V_{f,1}$	45.3(± 0.2%)	6.64(± 16.0%)	1.70(± 17.2%)	0.99
	$V_{f,2}$	49.1(± 0.1%)	5.80(± 4.0%)	1.26(± 2.4%)	−0.03
	$V_{f,3}$	53.1(± 0.3%)	4.16(± 12.2%)	0.907(± 14.0%)	1.30
13	$V_{f,1}$	45.2(± 0.1%)	6.80(± 8.9%)	3.11(± 16.8%)	4.29
	$V_{f,2}$	48.8(± 0.1%)	4.20(± 9.8%)	1.64(± 13.1%)	0.87
	$V_{f,3}$	52.7(± 0.2%)	2.62(± 4.9%)	0.714(± 10.6%)	0.70
14	$V_{f,1}$	46.0(± 0.3%)	10.7(± 6.8%)	1.23(± 5.8%)	0.96
	$V_{f,2}$	49.6(± 0.4%)	4.59(± 6.8%)	0.341(± 17.8%)	6.59
	$V_{f,3}$	53.6(± 0.2%)	3.57(± 15.9%)	0.304(± 50.2%)	4.38
15	$V_{f,1}$	46.1(± 0.1%)	7.24(± 10.1%)	1.23(± 9.9%)	7.21
	$V_{f,2}$	49.8(± 0.1%)	4.29(± 10.5%)	0.535(± 8.9%)	6.01
	$V_{f,3}$	53.5(± 0.2%)	3.21(± 8.8%)	0.315(± 14.0%)	2.39
16	$V_{f,1}$	46.0(± 0.0%)	7.19(± 5.4%)	1.16(± 2.6%)	−11.45
	$V_{f,2}$	49.7(± 0.0%)	4.94(± 6.8%)	0.698(± 9.9%)	−9.66
	$V_{f,3}$	53.7(± 0.1%)	3.24(± 4.5%)	0.601(± 4.0%)	−1.26
17a	$V_{f,1}$	46.1(± 0.0%)	5.94(± 3.9%)	1.29(± 5.9%)	0.40
	$V_{f,2}$	49.9(± 0.0%)	5.32(± 9.2%)	0.926(± 7.4%)	1.80
	$V_{f,3}$	53.8(± 0.0%)	4.45(± 5.4%)	0.838(± 9.8%)	2.00
17b	$V_{f,1}$	45.9(± 0.0%)	5.97(± 3.9%)	1.30(± 5.9%)	0.40
	$V_{f,2}$	48.3(± 0.0%)	5.50(± 9.2%)	0.957(± 7.4%)	1.80
	$V_{f,3}$	49.9(± 0.0%)	4.83(± 5.5%)	0.909(± 9.8%)	2.00
18	$V_{f,1}$	45.4(± 0.2%)	2.57(± 13.3%)	0.799(± 15.7%)	−2.69
	$V_{f,2}$	48.8(± 0.2%)	1.37(± 6.7%)	0.311(± 10.1%)	−3.45
	$V_{f,3}$	52.6(± 0.1%)	0.745(± 10.6%)	0.148(± 9.9%)	−3.66

(*continued on next page*)

Table 7 (*continued*)

Partici-pant #		fiber volume content in % (± c_v)	K_1 in 10^{-11} m^2 (± c_v)	K_2 in 10^{-11} m^2 (± c_v)	Orientation angle of K_1
19	$V_{f,1}$	47.5(± 0.3%)	133(± 18.7%)	30.8(± 59.4%)	8.52
	$V_{f,2}$	51.1(± 0.4%)	108(± 25.%)	30.2(± 79.4%)	−10.54
	$V_{f,3}$	54.9(± 0.7%)	126(± 20.6%)	23.6(± 17.4%)	0.66

[1] These values have been revised after first results presentation at FPCM14 as a data transfer error was identified by the participant.
[2] These values have been revised after first results presentation at FPCM14 as a unit conversion error was identified in the analysis software of the participant.

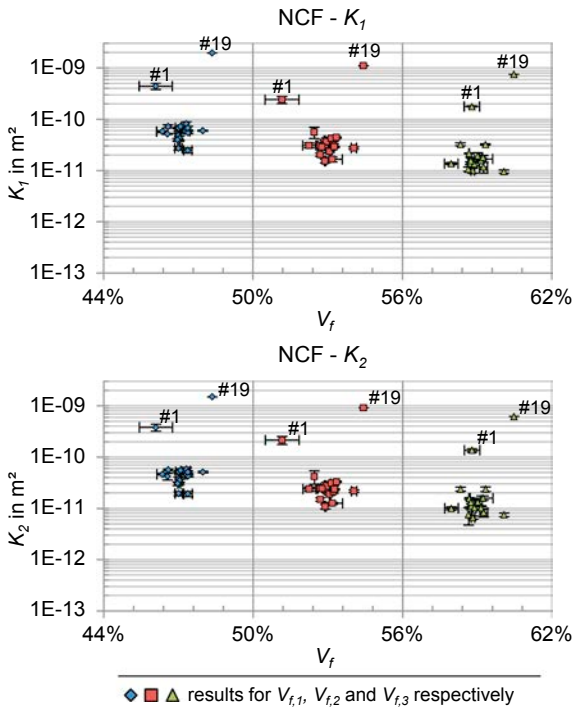

Fig. 5. Permeability results for the NCF. (For interpretation of the references to colour in this figure legend, the reader is referred to the web version of this article.)

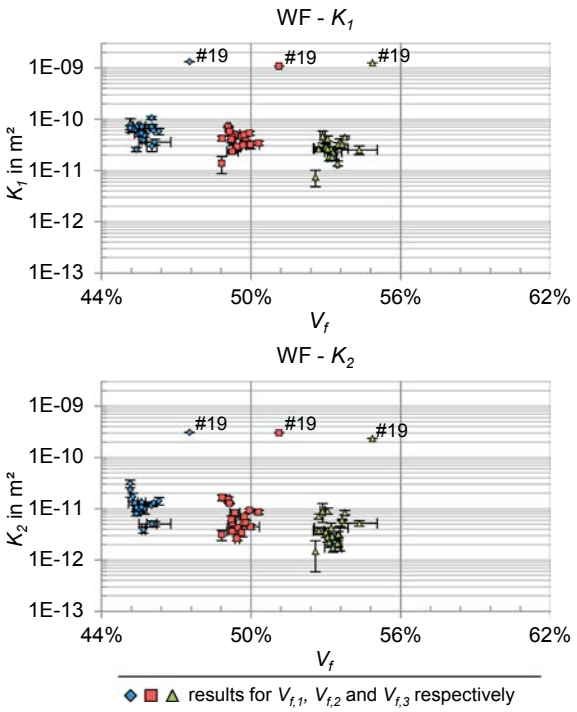

Fig. 6. Permeability results for the WF. (For interpretation of the references to colour in this figure legend, the reader is referred to the web version of this article.)

Firstly, the injection pressure itself might influence the permeability: Darcy's law assumes a rigid porous media. However, textiles can deform under the fluid pressure. Hence, it could make a difference which injection pressure is applied during permeability measurement, especially because of the very strong pressure gradient at the beginning of radial-flow experiments. All participants were asked to check the samples after testing for fiber-wash out and send photographs – no remarkable deformation was observed. Yet, if injection pressure is not properly set, it is presumed that the influence of fiber wash-out at the inlet can be remarkable since it may cause locally changed porosity and permeability and strong deviations from the expected pressure distribution. Also, as all participants were asked to use specific injection pressures, these effects should not contribute to deviations between the participant's results. Yet, the actual injection pressures were indeed not fully identical. Pressure loss in the feed line between the pressure vessel and the tool can cause deviations of the actual injection pressure from the target pressure set at the vessel. Even if this is taken into account for permeability calculation by using sensor data captured close to the injection point, this means the actual injection pressures among the participants varied. Yet, as the sensor values fairly accurately match the target values, this effect is estimated to be negligible for this benchmark. One of the 20 systems is based on a constant flow rate approach instead of constant injection pressure like the others. As the resulting data set was part of the cluster, this seconds the assumption that influence of injection pressure is negligible for this benchmark.

Secondly, pressure loss in the feed line between the sensor and the injection point can cause calculation errors. Within the benchmark, feeding line diameters and lengths from pressure sensor to injection point ranged from 4 mm to 12 mm and 50 mm to 5500 mm, respectively. At the given injection pressures, this can cause variation between the results. Also, analytically estimating the pressure loss in the feeding line is quite error-prone [10]. Further influence might be given by the fact that some participants use a pressure sensor value averaged over the complete test for permeability calculation, some use the single value of each time step and some average up all pressure values up to each time step.

All in all, since different influences contribute to variations, the benchmark results do not allow further statements. This would require tests with a focus on this influence.

Table 8
Coefficients of variation based on all data sets for the in-plane permeability values.

	NCF		WF	
	K_1	K_2	K_1	K_2
$V_{f,1}$	27.9%	27.3%	32.0%	50.4%
$V_{f,2}$	30.4%	29.9%	32.6%	56.2%
$V_{f,3}$	38.1%	39.6%	36.5%	55.7%
Average	32.2%	32.3%	33.7%	54.1%
	32.2%		43.9%	
	38.3%			

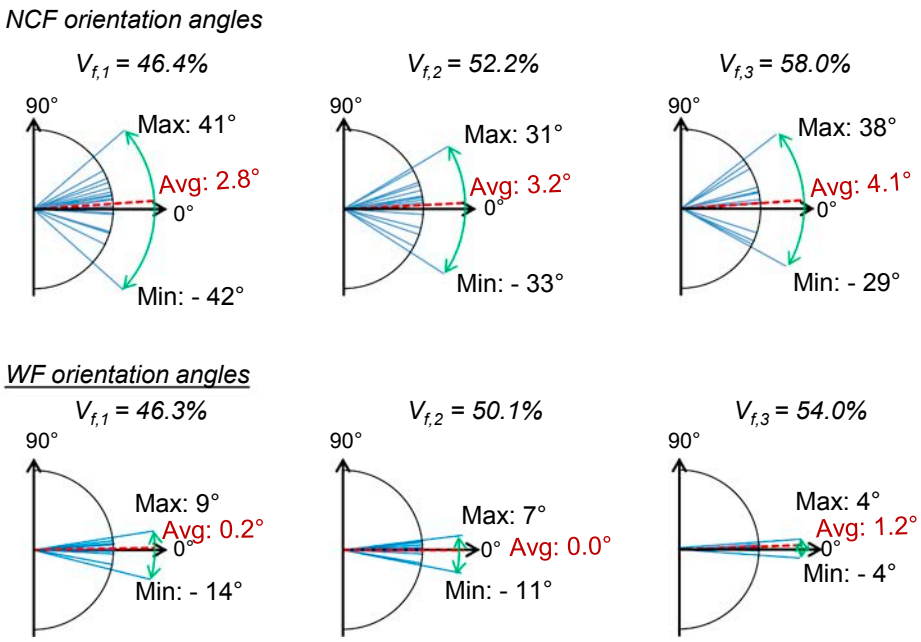

Fig. 7. Average orientation angles measured by the participants for the different target fiber volume contents; the dashed line shows the total average over all participants. (For interpretation of the references to colour in this figure legend, the reader is referred to the web version of this article.)

Table 9
Anisotropy values averaged over data of all participants and corresponding c_v.

	NCF		WF	
	K_2/K_1	c_v	K_2/K_1	c_v
$V_{f,1}$	0.78	6%	0.21	37%
$V_{f,2}$	0.78	9%	0.18	39%
$V_{f,3}$	0.75	10%	0.16	31%

Table 10
Normalized non-parallel cavity deformation.

Participant	1	2a	2b	3	4	5	6	7	8	9
ω in %	1.1	2.2	0.5	0.3	1.9	0.4	0.3	0.4	0.7	0.3
Participant	10	11	12	13	14	15	16	17	18	19
ω in %	0.5	0.1	0.3	4.7	0.6	0.7	0.0	1.0	0.6	7.7

4.3. Influence of fluid viscosity

Temperature-dependent viscosity is considered by all participants when calculating permeability via Darcýs law. Yet, there may be several sources of variation.

Opposing the assumptions underlying the application of Darcy‘s law, differences in viscosity could have secondary effects on the permeability, e.g. different deformation behavior of the preform or variations in wetting behavior. However, these influences are considered to be very small since the viscosity was in the range between 87 mPa·s and 113 mPa·s at temperatures between 17.3 °C and 27.4 °C, i.e. the temperature dependence is weak.

The viscosity for each single test is calculated using a viscosity-temperature function and the measured temperature. As can be seen in Table 2, participants measure the temperature at different locations: in the pressure vessel, the feed line, the tool, or in the laboratory. This can lead to differences between the temperature measured and the actual temperature of the fluid within the tool. Also, temperature might vary during the test as not all participants have air-conditioning systems that are used during the tests are performed. The data base does not allow a detailed statement about the influence of this effect.

Regional suppliers were selected for the silicone oil and the viscosity was centrally measured by Technische Universität München. The participants received the raw data of the measurements and individually fitted empirical functions to the viscosity-temperature data. At 23 °C, the measurement results of the batches showed an average variation of 1.7%. Yet, two participants measured the dynamic viscosity of the silicone oil with their own systems. The dynamic viscosity values at room temperature derived from the different functions applied in the benchmark, show a c_v of 3.8%. This indicates that additional uncertainty was induced by the diverse fitting functions.

Participant #1 received oil from a different batch than the other participants and measured the viscosity using their own equipment. Interestingly, the measured viscosity is the highest in the benchmark

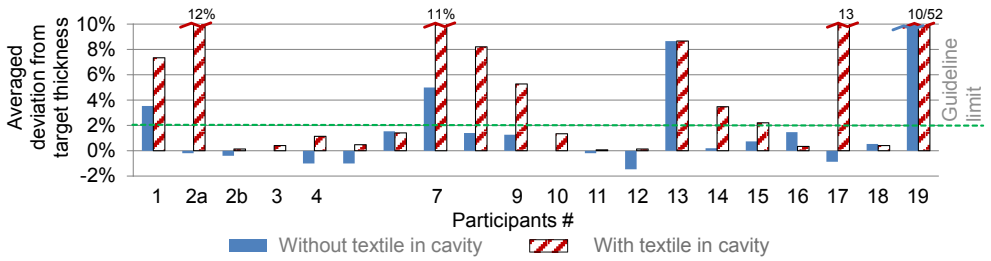

Fig. 8. Experimentally determined deviation of the cavity height from the target height. (For interpretation of the references to colour in this figure legend, the reader is referred to the web version of this article.)

study. This could be an actual difference of this specific batch, but it could also indicate that there is a systematic difference between the measurements carried out by TU München and by this participant. While this is speculative, it highlights a very important issue: Variations between the viscosity measurements performed on different systems will directly add to variations between permeability data measured at different research sites.

Even though it was tried to exclude influences of the viscosity, it presumably has an effect that is not negligible. Therefore, efforts for standardization of permeability measurement need to involve aspects of fluid-induced variations.

4.4. Influence of fluid wetting behavior

Silicone oil, as it was used in this benchmark, is a common substitute for resins in experimental studies of saturated and unsaturated permeability [8]. The choice of this type of fluid is based on its viscosity which is comparable to that of liquid epoxy resins used for composite manufacturing, the non-toxicity and the availability. However, so far capillary effects controlling wetting phenomena and potentially inducing void formation have been mostly neglected. Silicone oil is a totally dispersive liquid with a very low surface tension that makes it a totally wetting liquid. Uncured liquid epoxy resin, on the other hand, is a partially wetting fluid with a very different behavior, due to its surface tension and components thereof [25]. It is also impossible to consider a capillary pressure [26] for silicone oil. This could indicate that viscosity should not be the only parameter relevant to the choice of a non-reactive fluid as a substitute for liquid resin. Further studies should focus on the identification or formulation of a physico-chemically reliable test liquid for permeability measurements.

4.5. Influence of textile variations

Parts of the variation between the participants' data may be induced by textile variations. Fig. 9 shows the average areal weights measured for the test specimens by each participant. The error bars show the respective standard deviation. Although all material was from the same batch, some deviations between the participants exceed the variation for the single participants. However, the differences are relatively small and they were considered in calculating V_f. But variations in areal weight also indicate variations in the textile structure, such as straightening of yarns that would affect the crimp of the WF and would also influence the permeability.

Textile variation can also be seen on the level of the single yarns and bundles respectively, as the values listed in Table 3 show. Both textiles show variability in yarn/bundle width of about 5%. Based on common analytical models this alone can explain about 10% of the variability in terms of permeability. The cause for these variations may be related to the textile manufacturing process itself, to the rewinding procedures in the context of the material distribution, or to the individual lay-up and cutting procedures.

4.6. Influence of data analysis

Characterization of textile permeability basically comprises three steps: (1) Acquisition of relevant sensor data; (2) flow front modeling and allocation of pressure and viscosity values for each time step (eventually including time-averaging of pressure and viscosity values); and (3) computation of in-plane permeability data. Compared to linear injection tests, radial injection tests allow by far more variation in these steps, due to the more complex flow front shape and accordingly more complex mathematics. The 20 systems compared in the benchmark differ in terms of type, number and location of sensors for temperature, pressure and especially flow front monitoring (see Table 2). Accordingly, step (1) and (2) necessarily differ. Table 5 shows that the algorithms used for step (3) are also different.

The variations induced by the differences in steps (1) and (2) depend on the flow front shape. For an ideally homogeneous porous media, resulting in a perfectly elliptical flow front, it does not matter if the ellipse is fitted to several thousand values (optical systems) or only three (minimum when center is fixed), assuming that the sensor data is reliable. Yet, imperfections in the textile lead to local variations which can have a strong impact on measured permeability. This impact increases with decreasing number of sensors. Inaccuracy of flow front detection also induces variation. The distance of the sensors to the inlet can have an influence, as the inlet is circular, while the algorithms applied in step (3) assume that it is of the same shape as the flow front. This causes an error that decreases with increasing distance of the flow front to the inlet. Hence, it can make a difference where the sensors are located. This, however, was not examined in detail because the superposition of different causes of variation does not allow isolating

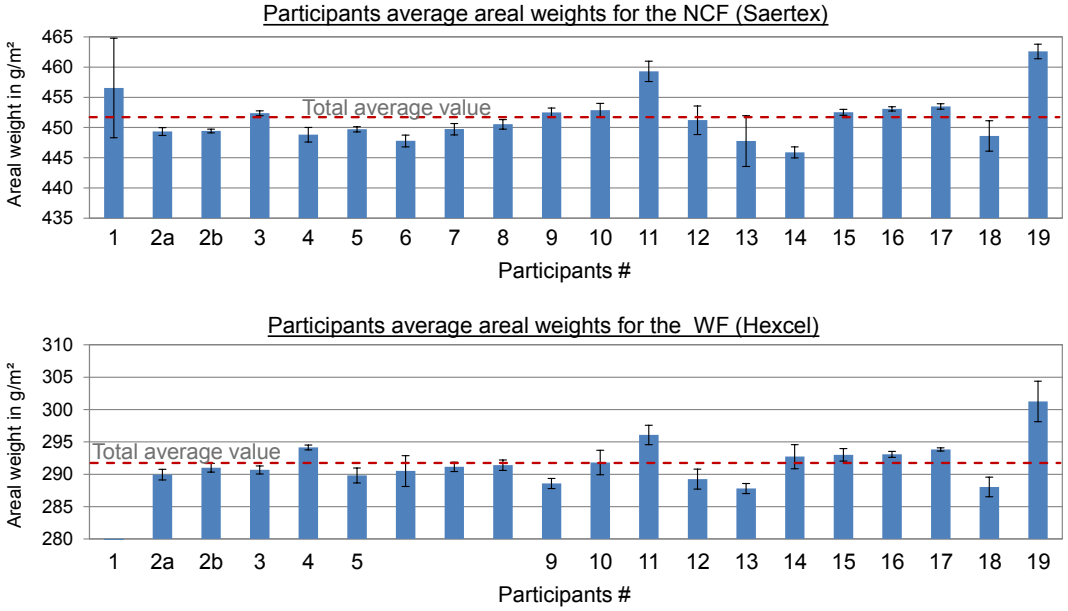

Fig. 9. Average areal weights measured for test specimens. (For interpretation of the references to colour in this figure legend, the reader is referred to the web version of this article.)

these effects.

Concerning the flow front modeling (step 2), two approaches exist for fitting an ellipse equation describing the flow front to sensor data. As illustrated in Fig. 10, the center of the fitted ellipse is either forced to coincide with the injection point, or the center is allowed to float. The floating center approach may lead to a better fit. But the algorithms used in step (3) are based on the assumption that flow spreads radially from the ellipse center and that the pressure has a maximum at this point. However, this is only true when the center of the ellipse coincides with the injection point [4]. It is evident that using different strategies can lead to variations. 4 out of 20 have used the floating center method.

The algorithms used for step 3 are known to show some differences when applied to the same data [4,27]. Additional variation can be induced by the strategy with which the algorithm is applied to the data. Four strategies can be distinguished (see also Ferland et al. [17]).

Elementary method: One of the permeability calculation algorithms is applied to the data of each pair of subsequent time steps and allows calculation of the permeability values based on the differences between the data sets at both time steps (esp. flow front progression). Hence, for each pair of subsequent time steps permeability values are obtained which can then be averaged to receive the final measurement values (K_1 and K_2) of the test.

Reference time step method: As with the elementary method permeability, values are calculated at each time step using one of the permeability calculation algorithms. Yet, not the difference to the previous time steps is considered, but always the difference to the very first time step (or another specific time step).

Single step method: Using one of the permeability calculation algorithms, the permeability is calculated with the data obtained at two particular time steps (e.g. the first and the last).

Global method: One of the permeability calculation algorithms is applied to the data of all time steps at once using a fitting procedure.

As listed in Table 5, 15 out of 20 stated the usage of global, 2 of elementary, 2 of reference time step and 1 of single step method. Some researchers had observed that the ellipse changes direction and shape based on which time step was used to collect the data, which might be caused by local variations. Such effects can cause a difference between the results gained with the above mentioned methods.

It is to be expected that significant variations origin from different methods for data analysis. In order to estimate the magnitude of variations induced by analysis it was decided to recalculate some of the results using a unified analysis approach. For this, the data sets (fluid injection pressure, dynamic fluid viscosity, flow front data) originally used in step (2) and (3) were collected and evaluated according to an uniform procedure: For step (2), the elliptic paraboloid fitting method introduced by Fauster et al. [9] was applied to all of the collected data sets, and for step (3), the Adams/Rebenfeld algorithm was used. As the paraboloid method allows fitting an elliptic paraboloid to the entire set of flow front data acquired during the radial flow experiments in a single step, it is a global method. Step (2) and (3) were performed at Montanuniversität Leoben for all collected data sets in order to minimize any influence related to data processing. This study was an additional offer to the participants, after the measurement phase of the benchmark study was concluded. Eight data sets (#2a, #2b, #5, #6, #7, #9, #12, #14, # 18) were recalculated this way.

To evaluate the influence of differences in step (2) and (3) on the final results, the in-plane permeability characteristics calculated with the individual approach (K_{1ind}, K_{2ind}, β_{ind}) can be compared with those calculated with the unified approach (K_{1uni}, K_{2uni}, β_{uni}). The relative deviation was calculated for each of the 15 tests for each participant, for both materials, and for K_1, K_2 and β (e.g. $\left|\frac{K_{1ind}-K_{1uni}}{K_{1uni}}\right|\cdot 100\%$). The average deviation and the corresponding standard deviations (minimum/maximum error bar) for each individual participant are shown in Fig. 11.

The deviations for the orientation angle of the NCF are significantly higher than those for the WF, which corresponds to the high variation of the orientation angle measurements described above. No clear trend was found for the difference between K_1 and K_2, neither for the NCF, nor for the WF. Also the results of the individual approach are not consistently higher or lower compared to the uniform approach. The average deviation for all the data shown in the diagram is 20% for K_1 and K_2 and 2° for β. This presumably corresponds to the magnitude of variation between the participants which is induced by the analysis. The total average coefficient of variation for K_1 and K_2 between the considered data sets is 43% when the individual approaches are applied and 36% when the uniform approach is applied. Hence, significant potential for further reduction of variation is possible.

5. Conclusions

The purpose of the presented benchmark exercise was to evaluate the comparability of in-plane permeability characteristics obtained using different measurement systems based on radial flow experiments, and to identify sources of variation. For this purpose, 19 participants with 20 systems measured the permeability of a non-crimp fabric and a woven fabric.

Averaged over all 12 test cases (highest and lowest in-plane permeability of two textiles at three levels of nominal V_f), the coefficient of variation (c_v) between the permeability values determined with the different system was 32% and 44% for NCF and WF, respectively. On the other hand, the average c_v for the individual systems was 8% and 12% for NCF and WF respectively, so the variation between systems is significantly higher than the uncertainty for a single system. Several causes for this difference were identified, leading to the conclusion that strategies to minimize differences in permeability values obtained using different systems will have to focus on these points:

- Cavity deformation is presumably the largest influence and strongly varies among participants. The results show that cavity deformation can be strongly reduced by appropriate design of the test set-up.
- There is no uniform strategy on where to measure injection pressure, which is might induce variation. A pressure sensor located at

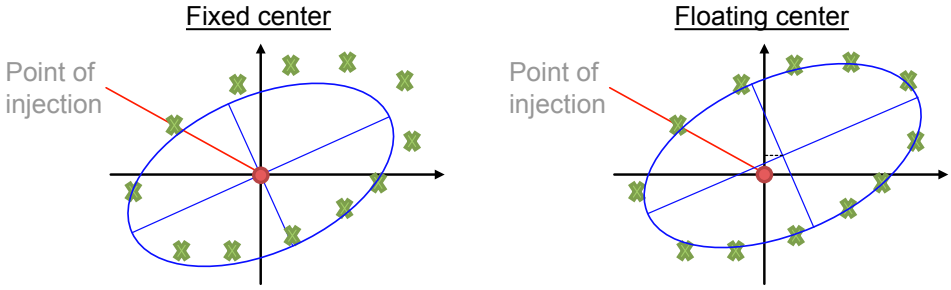

Fig. 10. Basic strategies for ellipse modeling – fixed center (left) and floating center (right). (For interpretation of the references to colour in this figure legend, the reader is referred to the web version of this article.)

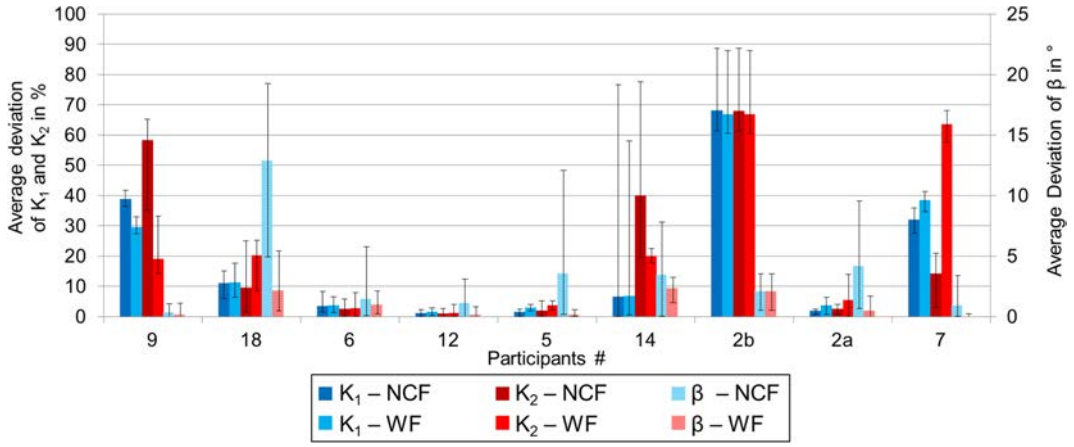

Fig. 11. Averaged deviations between results obtained using a unified and individual approach, respectively. (For interpretation of the references to colour in this figure legend, the reader is referred to the web version of this article.)

the injection gate will provide more consistency.

- Any effort to standardize permeability must take into account the methods to determine viscosity. Uncertainty in determination of the fluid viscosity, fitting of viscosity-temperature curves and temperature measurement can induce variation in the magnitude of several percent. Also it might help to find a model fluid whose viscosity is constant over a range of temperature and has good wetting properties.
- Stack-wise measurement of areal weight and calculation of corresponding fiber volume content should be mandatory to consider areal weight variations.
- Differences in the methods used for data analysis induce significant variation. A uniform data analysis tool could be created and used to eliminate the variation caused by the analysis method.

As a next step, the participants of the benchmark will derive some basic minimum requirements for permeability measurement systems and procedures (radial flow) from these results. Subsequently, smaller and topic-focused benchmarks will deal with remaining questions, e.g. the influence of injection pressure and the best strategy for injection pressure determination. Together with the first and second international benchmark exercise, the authors are confident that this will provide sufficient data for definition of guidelines for permeability measurement.

Acknowledgement

It is kindly acknowledged that the textile manufacturing companies Saertex GmbH and Hexcel Corporation supported the benchmark by supplying the materials free of charge.

References

[1] Parnas RS, Flynn KM, Dal-Favero ME. A permeability database for composites manufacturing. Polym Compos 1997;18(5):623–33.
[2] Parnas RS, Howard JG, Luce TL. Advani SG. Permeability characterization. 1. A proposed standard reference fabric for permeability. Polym Compos 1995;16(6):429–45.
[3] Lundström TS, Stenberg R, Bergstrom R, Partanen H, Birkeland PA. In-plane permeability measurements: a nordic round-robin study. Compos A Appl Sci Manuf 2000;31(1):29–43.
[4] Fauster E, Berg DC, Abliz D, Grössing H, Meiners D, Ziegmann G, et al. Image processing and data evaluation algorithms for reproducible optical in-plane permeability characterization by radial flow experiments. J Compos Mater 2017. 0021998318780209.
[5] Grössing H, Becker D, Schledjewski R, Mitschang P, Kaufmann S. An evaluation of the reproducibility of capacitve sensor based in-plane permeability measurements: a benchmarking study. eXPRESS Polym Lett 2015;9(2):129–42.
[6] Arbter R, Beraud J, Binetruy C, Bizet L, Bréard J, Comas-Cardona S, et al. Experimental determination of the permeability of textiles: a benchmark exercise. Compos A Appl Sci Manuf 2011;42(9):1157–68.
[7] Alms JB, Correia N, Advani SG, Ruiz E. Experimental procedures to run longitudinal injections to measure unsaturated permeability of LCM reinforcements. Permeability measurement standard, permeability benchmark II; 2010. http://cchpmeca polymtl ca/permeabilityBenchmarkII html.
[8] Vernet N, Ruiz E, Advani S, Alms J, Aubert M, Barburski M, et al. Experimental determination of the permeability of engineering textiles: benchmark II. Compos A Appl Sci Manuf 2014;61:172–84.
[9] Fauster E, Berg DC, May D, Blößl Y, Schledjewski R. Robust evaluation of flow front data for in-plane permeability characterization by radial flow experiments. Adv Manuf Polym Compos Sci 2018;4(1):24–40.
[10] Berg D, Fauster E, Abliz D, Grössing H, Meiners D, Schledjewski R, et al. Influence of test rig configuration and evaluation algorithms on optical radial-flow permeability measurement: a benchmark exercise. Proc 20th int conf on composite materials, Copenhagen, Denmark. 2015.
[11] Kissinger C, Mitschang P, Neitzel M, Roder G, Haberland R. Continuous on-line permeability measurement of textile structures. Bridging the centuries with Sampe's materials and processes technology, vol. 45, Books 1 and 22000. p. 2089–96.
[12] Aranda S, Berg D, Dickert M, Drechsel M, Ziegmann G. Influence of shear on the permeability tensor and compaction behaviour of a non-crimp fabric. Compos B Eng 2014;65:158–63.
[13] Swery EE, Allen T, Comas-Cardona S, Govignon Q, Hickey C, Timms J, et al. Efficient experimental characterisation of the permeability of fibrous textiles. J Compos Mater 2016;50(28):4023–38.
[14] Louis BM, Di Fratta C, Danzi M, Zogg M, Ermanni P. Improving time effective and robust techniques for measuring in-plane permeability of fibre preforms for LCM processing. New material characteristics to cover new applications needs: SEICO 11; SAMPE. Europe 32nd international technical conference & forum; march 28th–29th, 2011, Paris; proceedings 2011 SAMPE Europe international conference Paris: society for the advancement of material and process engineering. 2011. p. 204–11.
[15] Alhussein H, Umer R, Rao S, Swery E, Bickerton S, Cantwell W. Characterization of 3D woven reinforcements for liquid composite molding processes. J Mater Sci 2016;51(6):3277–88.
[16] Endruweit A, McGregor P, Long A, Johnson M. Influence of the fabric architecture on the variations in experimentally determined in-plane permeability values. Compos Sci Technol 2006;66(11–12):1778–92.
[17] Ferland P, Guittard D, Trochu F. Concurrent methods for permeability measurement in resin transfer molding. Polym Compos 1996;17(1):149–58.
[18] Adams KL, Rebenfeld L. Permeability characteristics of multilayer fiber reinforcements. 1. Experimental-observations. Polym Compos 1991;12(3):179–85.
[19] Chan AW, Hwang ST. Anisotropic in-plane permeability of fabric media. Polym Eng Sci 1991;31(16):1233–9.
[20] Adams KL, Miller B, Rebenfeld L, Hwang ST, Chan AW. Forced inplane flow of an epoxy-resin in fibrous networks. Polym Eng Sci 1986;26/20(20)::1434–41.
[21] Adams KL, Rebenfeld L. Permeability characteristics of multilayer fiber reinforcements. 2. Theoretical-model. Polym Compos 1991;12(3):186–90.
[22] Adams KL, Russel WB, Rebenfeld L. Radial penetration of a viscous-liquid into a planar anisotropic porous-medium. Int J Multiph Flow 1988;14(2):203–15.

[23] Weitzenböck J, Shenoi R, Wilson P. Radial flow permeability measurement. Part A: Theory. Compos A Appl Sci Manuf 1999;30(6):781–96.
[24] Weitzenböck J, Shenoi R, Wilson P. Radial flow permeability measurement. Part B: Application. Compos A Appl Sci Manuf 1999;30(6):797–813.
[25] Pucci MF, Liotier P-J, Drapier S. Tensiometric method to reliably assess wetting properties of single fibers with resins: Validation on cellulosic reinforcements for composites. Colloids Surf A 2017;512:26–33.
[26] Pucci MF, Liotier P-J, Drapier S. Capillary wicking in a fibrous reinforcement–orthotropic issues to determine the capillary pressure components. Compos A Appl Sci Manuf 2015;77:133–41.
[27] Fauster E, Grössing H, Schledjewski R. Materials ESoC. Comparison of algorithms for 2D anisotropic permeability calculation in terms of uncertainty propagation. European Society of Composite Materials). Proc 16th eur conf of composite materials Seville, Spain. 2014.
[28] Meier R, Walbran A, Hahn C, Zaremba S, Drechsler K. Methoden zur Bestimmung der Permeabilität von Verstärkungstextilien. J Plast Technol 2014;10.